Original Research Paper

Effect of fabrication method on the structure and properties of a nanostructured nickel-free stainless steel

L. Heidari [a], A. Tangestani [a,*], M.J. Hadianfard [a,*], D. Vashaee [b], L. Tayebi [c]

[a] Department of Materials Science and Engineering, School of Engineering, Shiraz University, 71348-51154 Shiraz, Iran
[b] Electrical and Computer Engineering Department, North Carolina State University, Raleigh, NC 27606, USA
[c] School of Dentistry, Marquette University, Milwaukee, WI, 53233, USA

ABSTRACT

An ASTM F2581 nanostructured stainless steel was fabricated by two different powder metallurgy routes; Hot Powder Forging (HPF) and Binder Assisted Extrusion (BAE) methods. Their structure and mechanical properties were investigated and compared. In both fabrication methods, the alloy powder was made by using main alloying elements through mechanical alloying, along with the addition of a sintering aid. In the BAE method, a paste was prepared by mixing alloy powders with polymer followed by cold extrusion, polymer removal, and sintering. In the HPF method, the alloy powders were hot forged under high pressure. The structure and the size of the austenite crystallite of the samples were investigated by scanning electron microscopy (SEM), FE-SEM, x-ray diffraction (XRD) and transmission electron microscopy (TEM). It was determined that the samples prepared by the HPF method are generally denser than those made via BAE. The porosities are smaller and almost uniform in size and morphology in the HPF method. Furthermore, microhardness and tensile tests were performed on the samples. The results show that the ductility of BAE samples is higher than the HPF samples. The fracture surface of the BAE sample has deeper dimples, indicating higher ductility for BAE samples. On the other hand, both the hardness and strength of HPF samples are higher than those of the BAE samples. The results show that both methods produced specimens with considerably higher strength and hardness than conventional 316L stainless steel.

© 2020 The Society of Powder Technology Japan. Published by Elsevier B.V. and The Society of Powder Technology Japan. All rights reserved.

1. Introduction

Most orthopedic implants are currently produced from three groups of the iron-base, cobalt-base, and titanium-base alloys. Iron base alloys have a lot of applications due to their various manufacturing methods, high strength and ductility, biocompatibility, and low cost [1,2]. The structure of iron-base stainless alloys is divided into four groups, including ferritic, austenitic, martensitic, and duplex. Duplex stainless alloys have no application in the medical field, and ferrite stainless steel is also limited in the use of medical devices, however, martensitic stainless steels are used for dentistry and surgical equipment manufacturing [3]. Among the four groups of stainless steels, austenitic stainless steels are the most widely used in the manufacturing of orthopedic implants and production of surgical equipment because of features such as high formability,

high corrosion resistance and biocompatibility [4]. As a result, austenitic stainless steel is only used in the manufacturing of temporary implants. Nickel-free austenitic stainless steels were introduced to remove this defect [5]. In these alloys, the nitrogen is used instead of nickel to stabilize the austenite phase. Nitrogen causes a decree in cavity corrosion, reduced grain size, and increased strength [6–9]. The alloy investigated in this study is high nitrogen austenitic stainless steel ASTM F2581. In general, materials used as orthopedic implants should have the characteristics of non-toxicity, high compatibility, and mechanical properties such as Young's modulus, strength, and hardness close to the bone. In cases where the modulus of implants is higher than the Young's modulus of the bone, there is a stress shielding effect that causes implant placement. Other factors that cause bone loss include the reduction of abrasion resistance and low bone ability [10]. The fabrication method has a considerable effect on the mechanical properties of the material. Today attention has been paid to the production of materials that have simultaneous high strength and high ductility. These materials have advantages in the

---

manufacturing of orthopedic implants. There are various fabrication methods such as casting and powder metallurgy, to produce orthopedic implants [11]. Orthopedic implants produced by conventional methods such as casting have the strength and Young's modulus higher than bones, as stated, which causes a shielding effect. In powder metallurgy, the materials produced have sufficient strength and lower Young's modulus. In this method, porosity reduces the Young's modulus of the implant that approaches that of bone, and also porosities increase tissue growth on the surface of the implant [12–14]. There are different methods for the part manufactured via powder metallurgy including press and sintering, powder extrusions [15], binder assisted extrusion (BAE) [16], hot powder forging (HPF) [17,18], hot isotactic pressing (HIP) [19], cold isotactic pressing (CIP) [20], and hot powder rolling (HPR) [21]. The CIP and HIP methods are not cost-effective due to the need for expensive equipment as well as the small sample size. HRP is also a method with sophisticated and costly equipment. The hot extrusion method has no dimensional limitation for component production, but it also requires a standard mold and strong press due to its high pressure and temperature. Therefore, in this study, the BAE and HPF methods are used to make high nitrogen Nickel-Free Austenitic Stainless Steel.

The BAE method is another powder metallurgy process in which a binder facilitates the formability of the powders and makes it possible to produce green samples in the cold state [22,23]. For this purpose, a polymer binder is needed to hold the primary powder particles together and the extrusion process to be carried out at room temperature and low pressure up to 50 MPa [24,25]. BAE is also one of the techniques to form ceramics [26]. It is challenging to develop ceramic parts by powder metallurgy because the ceramic powders are non-plastic and require additives to facilitate the movement of the powders. Therefore, researchers introduced binders that were added to the ceramic powder to obtain a well-shaped paste and could be comfortably cold extruded to form samples [27]. Another method that is used in this study for investigation is the HPF. In this method, compressive strain and lateral flow at high temperatures cause dynamic recovery [28]. This phenomenon reduces grain size and also increases ductility. Porous implants are divided into two categories: First, implants whose cavities are located only on their outer surface, and second, Implants in which cavities are distributed on the surface and inside. The first category is produced by using plasma spray, acid treatment, and sandblasting methods. In these methods, the cavities only increase the adhesion between the tissue and the implant, but Young's modulus does not affect. The second category is produced by powder metallurgical routes, etc.in this case the adhesion between tissue and implant increases, and, also Young modulus of the material can be adjusted to the required point. For the production of this group, in some powder metallurgy methods, a space holder is used to produce porous materials. In these methods, a probability of increasing contamination inside the alloy is serious and it is not recommended for medical applications [29]. HPF
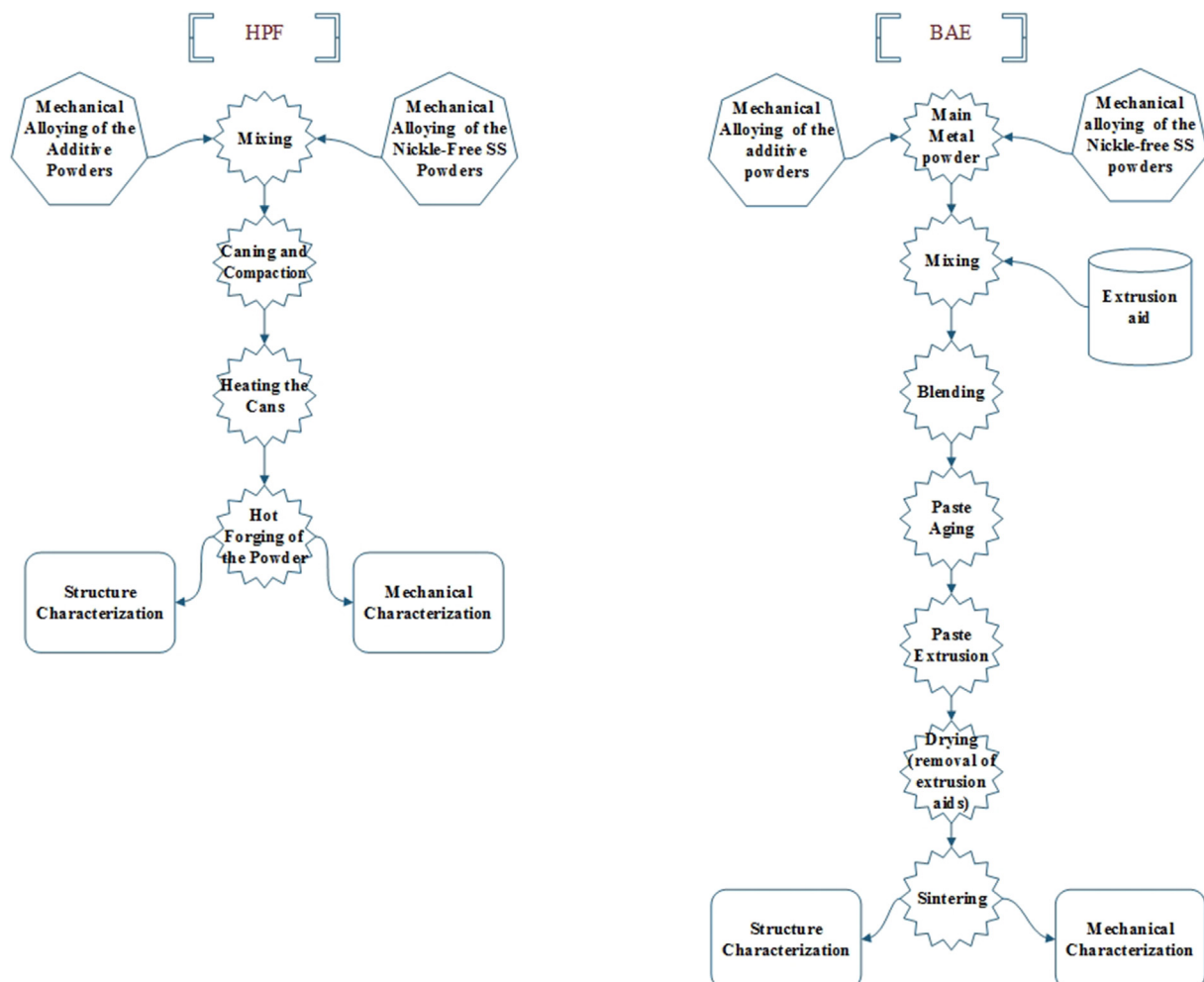

Fig. 1. A schematic of HPF and BAE fabrication methods.

Table 1
Chemical composition of the Nickel-Free Stainless Steel (wt %).

Element	Cr	Mn	Mo	Si	C	N	Fe
Content (wt. %)	17	10	4	0.4	0.2	0.5	Bal.

Table 2
Extrusion parameters for binder assisted extrusion method.

Extrusion pressure (MPa)	Hole diameter (mm)	Extrusion angle	Length of die (mm)	Extrusion ratio	Extrusion speed (mm/min)
5	4	90	10	10	1

and BAE Methods are capable to produce porous materials without using a space holder. As yet, numerous studies have been done on various alloys made by the HPF method. In this research, the microstructure and mechanical properties of Fe-C-Cu alloy produced by HPF were investigated. The results showed that the HPF method produced strengthening mechanisms such as grain refinement and precipitation hardening in the alloy [30]. The microstructure of biocompatible Ti-Mn steel made by HPF was also investigated. The results showed that the HPF method eliminates porosity and increases the density of the fabricated alloy [31]. Zhang et al. studied the properties of high-alloy and low-alloy Mo-Mn-Si-C steel made by HPF. The results showed that the highest tensile strength and the least dimension change were achieved in the low alloy steel [32]. Bai et al. studied the mechanical properties of nickel superalloy made by HPF. The results showed that in the alloy made by the HPF method, the density at the center of the alloy was higher than that of the alloy edge. The results also showed that by increasing the compressive stress on the powders, the alloy would be fully dense [33]. However, so far, no studies have been performed on nickel-free austenitic stainless steel fabricated by HPF. There are differences between the two methods of fabrication. In the BAE method, the raw sample is produced at room temperature and low pressure, then sintered at high temperature. But in the HPF method, high temperature and pressure are applied during the sample construction, which creates dislocations in the structure. Also, because of the force applied to the powders, the sample has less porosity [34,35]. In this study, the ASTM F2581 alloy, which was fabricated by HPF and BAE methods, are compared in terms of physical and mechanical properties.

2. Material and methods

A schematic of the austenitic stainless steel fabrication steps in HPF and BAE methods is presented in Fig. 1.

2.1. Powder preparation

Powders used in HPF and BAE methods are similarly prepared by mechanical alloying. The chemical composition of the powders is shown in Table 1. For addition of nitrogen to the alloyed powders, rather than nitrogen gas, Fe_3N was utilized. This method has already been investigated by our research team. A biocompatible additive (Mn-11.5 wt% Si) was used to decrease sintering temperature. Salahinejad and Javanbakht have proven that this sinter aid leads to improved microstructural and mechanical properties [36]. Due to the similarity of the chemical composition of the powder in the present study with our previous work [37], 6 wt% of additive was selected as the optimum amount for adding to the stainless steel powder. The additive powder (Mn–11.5 wt% Si) is also made by mechanical alloying. Further details of the powder preparation are presented in Ref. [38].

2.2. Sample preparation

2.2.1. Hot powder forging

In the HPF fabrication method, the prepared powders from the mechanical alloying process were poured into a stainless steel 316 cylindrical can. The powders were compressed under 40 MPa. then, the can was sealed to prevent oxidation of the powders. The can containing the powders was placed into the furnace for 2 h at 1200 °C and was immediately forged under 2 GPa by a hydraulic press. After the forging process, the sample was cooled at room temperature.

2.2.2. Binder assisted extrusion

For paste preparation, 94 wt% of stainless steel powder, 3 wt% of binder, 2 wt% of plasticizer, 1 wt% of dispersant and cyclohexane as a solvent were mixed. In this system, polyvinyl pyrrolidone (PVP) was utilized as a binder, ethylene glycol, as a plasticizer and stearic acid as the dispersant. The solvent powder, binder, and plasticizer were uniformly mixed to produce the paste. The mixing was done by a magnetic shear mixing system at 100 rpm. Then the paste was cold extruded at room temperature. The cold extrusion parameters are listed in Table 2.

The extruded samples were then placed in an argon furnace to remove the binder. The furnace temperature was raised to 550 °C at a rate of 1 °C/min and maintained at this temperature for 2 h. After removing the binder, the sample was sealed in a vacuum medium in the quartz chamber and sintered for 1 h at 1150 °C. The samples were then quenched in water to obtain austenitic structure.

2.3. Structural characterization

To investigate the structural-phase of the samples, x-ray diffraction analysis by Cu kα with $\lambda = 0.15406$, step size 0.05, and step time 1 s was used. MAUD (Version 2.26) program was used to analyze x-ray diffraction data. In this software, the Reitveld estimate was used to calculate the percentage of phase and the double-Voigt approach to calculate crystallite size [39]. The steel samples were polished to 100 μm thickness and then electro-polished to under 1 μm thickness for subsequent preparations for the TEM analysis. Also, the LECO gas analysis method was used to measure the nitrogen content of the samples.

2.4. Physical characterization

To prepare the specimens for scanning electron microscopy, the surface of the samples were polished and etched with a 60% nitric acid solution. The microstructure of the specimens before and after the etching was investigated by FE-SEM and SEM. Also, the density of the samples was measured by the Archimedes immersion method.

2.5. Mechanical properties

The microhardness test of the samples was measured by the Vickers hardness test. The average of the five measurements was reported as the microhardness value. To measure the yield strength, the ultimate tensile strength (UTS) and the ductility of the samples, the tensile tests were performed at room temperature. An INSTRON-8802 device with a strain rate of 0.1 mm/s was used for these tests, and the specimens were made according to the ASTM E-9 standard.

3. Results and discussion

The phases in the two samples were analyzed by XRD. The XRD results for two different samples produced with the various fabrication methods are shown in Fig. 2.

Peaks and the related crystalline planes shown in the XRD patterns are linked to the austenitic iron structure of the two samples. The crystallite size and phase percentages are calculated by Rietveld analysis of the XRD results. Although in the XRD pattern, the peak that represents the ferrite phase was not observed, in the Rietveld analysis, more than 99% austenitic and less than 1% of ferrite, phases have been identified in both specimens. This calculation shows that nitrogen atoms could produce a stable austenitic phase in both specimens. Since the specimens are almost entirely austenitic phase, they are perfectly suitable for implant manufacturing [40,41]. The crystallite sizes determined by the XRD analysis are 90 nm for the BAE specimen and 62 nm for the HPF specimen. It is well known that by developing a grain refining process, a significant improvement in mechanical properties like strength, fracture, and fatigue behavior is attainable.

Fig. 3a and c show TEM image of the BAE and HPF samples respectively, The SAD patterns representing the nanocrystalline structure of both samples are presented in Fig. 3b and d. Due to the high strain applied to the powders during mechanical alloying, a large number of dislocations are formed in the powders. These dislocations arrange the subgrains, which produce powders with nanocrystalline structure. These results indicate that the sample fabricated by both BAE and HPF methods retain their nanostructure even after high-temperature treatment during fabrication, and their grain did not grow to the micron size. A previous investigation on this alloy also showed that the nanocrystalline structure reminds stable during high-temperature sintering [37]. Nitrogen and carbon are interstitial elements that segregate at the grains boundaries and by locking dislocations, prevent grain boundary movement and grain growth [42]. The results of nitrogen analysis by the LECO gas analyzer show that only 0. 01 wt% of nitrogen was lost during the high-temperature treatments of the samples.

In the SAD pattern, bright spots on the rings represent the planes of the nanosize crystal. The SAD of the HPF sample (Fig. 3d) has more bright spots than the BAE sample (Fig. 3c). This indicates that the number of the crystalline planes of the HPF samples is more than that of the BAE sample; therefore, the SAD analysis has determined the size of the crystallites in HPF samples is smaller than the BAE samples.

Fig. 4 displays the back scattered-electron (BSE) imaging of the HPF and BAE samples without etching. These figures show the distribution of the sintering aid in the specimens and indicate a more uniform distribution of the sintering aid in the HPF method.

Fig. 5 shows the optical image of the specimens for both HPF and BAE methods before and after etching. These figures show the size, shape, and distribution of the porosities and distribution of the sintering aid around the powder particles.

The percentage and data about the morphology of the porosities were calculated using image analyzer software. The results are shown in Fig. 6a and Table 3.

According to these results, the porosities in the BAE sample are 2.41% more than the HPF sample. Also, the size range of the porosities in the BAE sample is larger than the HPF sample. In other words, in the HPF sample, the porosities are smaller and distributed more uniformly in the sample. The SEM and the optical images also exhibit that sintering aid in the HPF sample is distributed more evenly among the powder particles. These results confirm the superior structure of the HPF sample. Since the melting point of the sintering aid is around 1040 °C[36], at forging temperature under high pressure, it acts like a paste, fills the porosities quickly, distributes more consistently, and leaves fewer pores with smaller size. In the BAE method pressure and temperature applies to the specimen at a different time and separately. Therefore, primary particles cannot deform and fill the space between them by
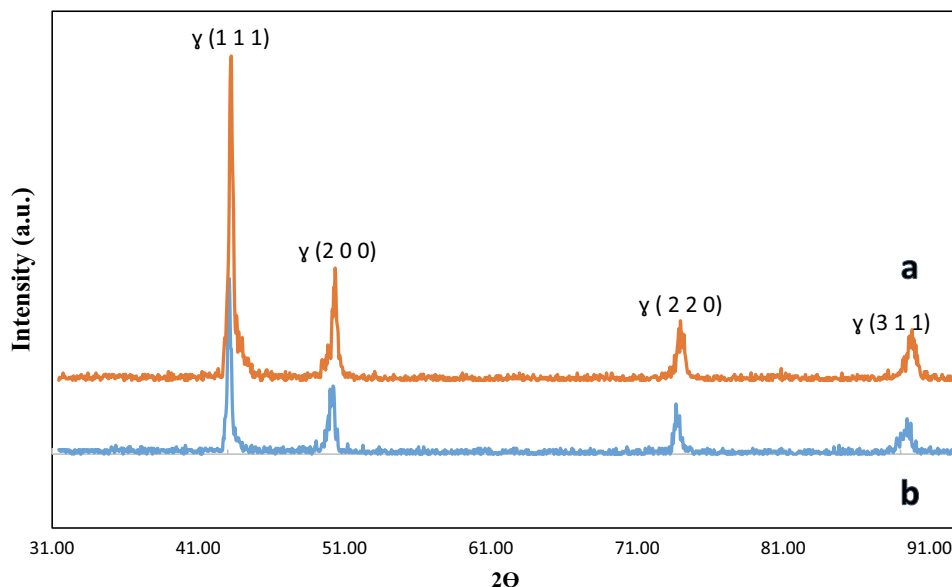

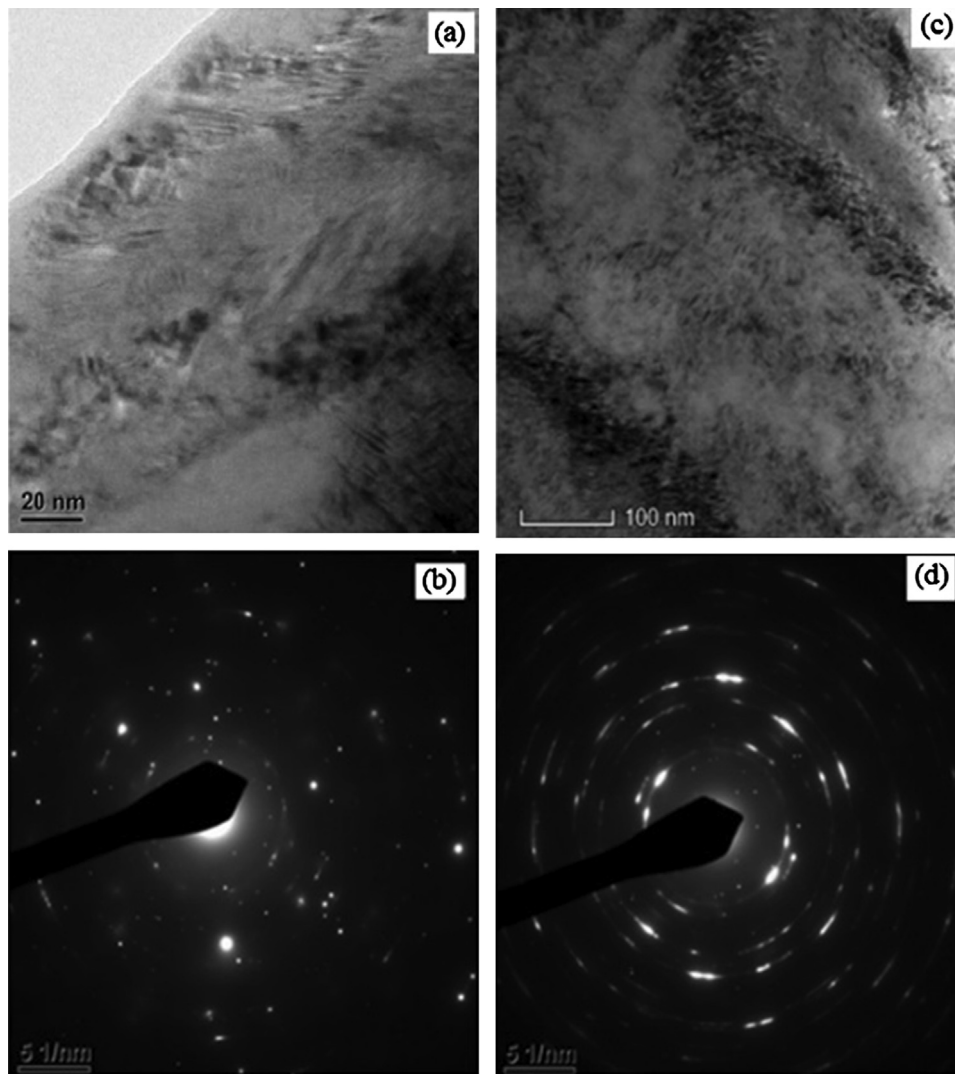**Fig. 2.** The XRD results for (a) HPF and (b) BAE samples.

Fig. 3. (a) TEM image and (b) SAD pattern of the BAE sample, and (c) TEM image and (d) SAD pattern of the HPF.
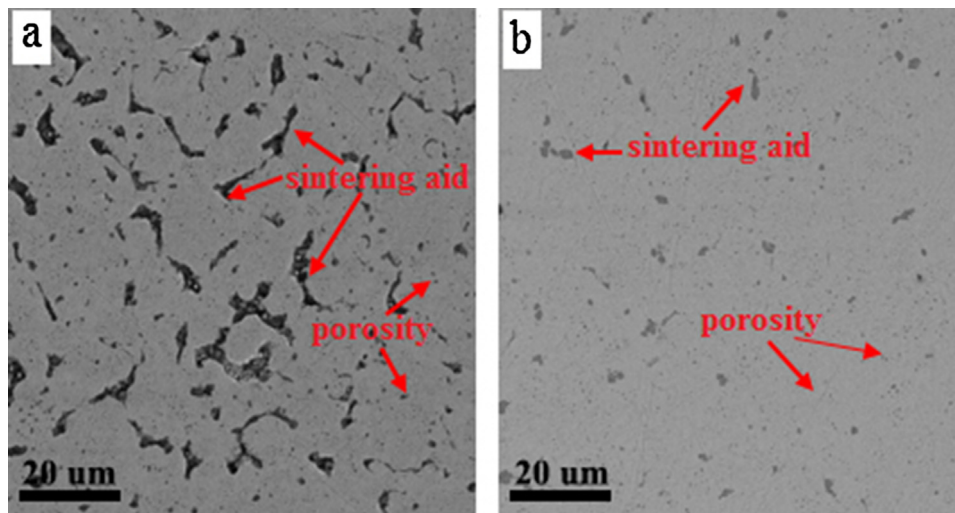

Fig. 4. SEM-BSE image of the specimens without etching (a) BAE sample and (b) HPF sample.

applying the pressure, and densification occurs at high temperatures due to liquid sintering and diffusion of the liquid phase into the porosities and between the particles. In the HPF method, pressure applies to the specimen when it is hot, in this
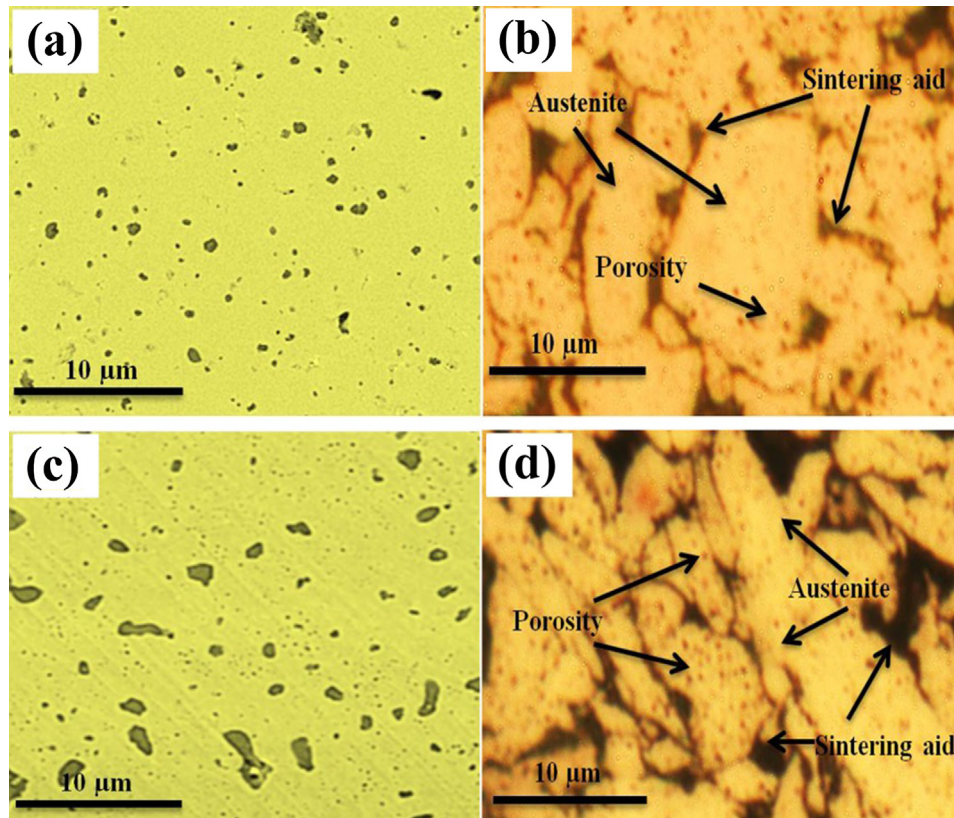
Fig. 5. Optical microscope image of (a) HPF before etch, (b) HPF after etch, (c) BAE before etch and (d) BAE after etching.

case at the same time two incidents are happening. Frist the sintering aid, which is pasted flows to the porosities between the particles under high pressure and fills their space well. Second stainless steel particles at high temperature deform and flow into the available spaces between them. Therefore, under high pressure and temperature all, the primary powders migrate or deform and stick together, as a result, the space between the particles dwindles and the density of the sample increases. This process provides mainly closed and unconnected holes in the HPF sample. This feature prevents the penetration of corrosive substances into the implant during service application and increases the life of the implant in the corrosive environment. Besides, dynamic recrystallization occurs in the HPF sample under high pressure and temperature condition. Since in the nickel-free stainless steel, the amount of stacking fault energy (SFE) is low, dynamic recovery of dislocations can occur easily. This feature increases the heterogeneous deformation property of fabricated alloy [43]. Consequently, the HPF method, in addition to making porous materials that are suitable for orthopedic applications, the grain refinement process is also performed in the structure, which leads to creating superior properties over the BAE sample.

The relative density of samples fabricated by the HPF and BAE method obtained by the Archimedes method is shown in Fig. 6-b. The density of the HPF sample is 3% more than the BAE sample. In the HPF method, due to the high applied pressure at the sintering temperature, a greater connection occurs between the particles, and the high pressure leads to the penetration of the particles into each other, resulting in high densification of the samples.

Fig. 6(c, d) illustrates the FE-SEM image of samples after etching. As seen in Fig. 6(c, d), the powders are well connected together. This indicates that the samples are sintered completely. The results of the microhardness test are shown in Fig. 7a. The

microhardness of the samples was measured by the Vickers hardness test. The hardness of the HPF sample is 17.7% more than the BAE sample. As shown in Fig. 7a, the microhardness of the nickel-free stainless steel, made by BAE and HPF fabrication method, is more than twice of the microhardness of an ordinary 316L austenitic stainless steel (SS). This higher hardness may be attributed to the nanosize structure of the nickel-free specimens [44].

Fig. 7b shows the stress–strain curve of the specimens obtained from the tensile test of alloys fabricated with HPF, BAE and ordinary 316L. During the test, the HPF and BAE samples show a uniform elongation with a sudden failure without exhibiting any macroscopic necking. HPF and BAE specimens show a large and well-defined plastic area. The HPF specimen indicates a higher elastic modulus with higher strengths. This behavior is related to a lower percentage of the porosities and also a smaller size. A comparison between yield strength (YS) and ultimate tensile strength (UTS) and ductility of the specimens and an ordinary 316L stainless steel is presented in Fig. 7c, d and e, respectively. The results indicate that the mechanical properties of the HPF sample are superior to the BAE sample. These results show that the HPF sample has a 16% higher YS and 19.9% higher UTS than the BAE sample. The tensile test results also show that the YS of the BAE sample is more than 2.8 times and the HPF sample is more than 3.2 times greater than the YS of an ordinary 316L stainless steel. However, according to Fig. 7e, the ductility of HPF and BAE samples is lower than 316L. Reduction in grain size leads to increase strength (according to Hall-Patch relation). On the other hand, ductility decreases [45,46]. In alloys, ductility is also dependent on the fabrication method. For example, at the same grain size, nanostructured aluminum produced by the severe plastic deformation method has higher ductility than the same alloy made by powder metallurgy [46]. Lower ductility in alloys produced via powder metallurgy is
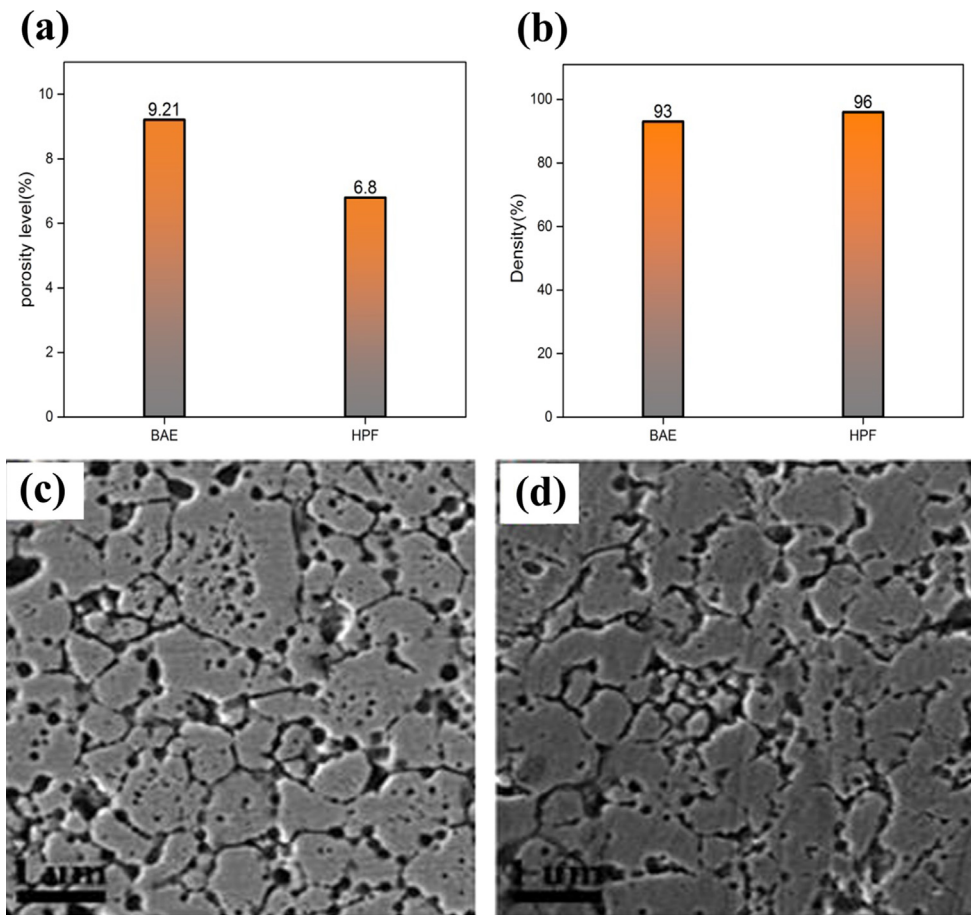
Fig. 6. A) Percentage of the porosity, obtained from image analysis BAE and HPF sample. B) Percentage of density BAE and HPF sample. C) FE-SEM images of the specimens after etching for BAE sample. D) FE-SEM images of the specimens after etching for HPF sample.

Table 3
Morphological data of the porosities for BAE and HPF samples.

Sample	Mean Size of Holes (μm)	Median Size of Holes (μm)	Size Range of Holes (μm)	Largest Hole Size (μm)	Standard deviation±(μm)
BAE	4.9	5.29	2.9–8.6	8.6	2.9
HPF	1.6	1.5	0.95–2.1	2.1	0.4

due to several reasons. Firstly, creation defects such as porosity or free space between powders during the fabrication process and secondly, lower dislocation mobility (ρm). It is stated that in the alloys produced by powder metallurgy dislocation mobility is low [47]. Although the BAE and HPF specimens show lower ductility compare to conventional 316L stainless steel, their ductility is about 20% which makes them ductile materials. This ductility together with very high strength and hardness performs them very suitable materials for high strength- high ductility applications.

The XRD results and TEM images provide evidence for the nanosize structure of both specimens. Moreover, it is known that during mechanical alloying, a large concentration of dislocations is created [47]. Therefore, one may relate the superior mechanical properties (more than two-fold) of the tested samples over the ordinary 316 stainless steel through these phenomena. Two strengthening mechanisms may account for the creation of this superior behavior in the specimens grain boundary strengthening and dislocation strengthening [48]. Hall Petch Effect, also known as grain boundary strengthening (equation1), refers to a phenomenon of increasing the tensile strength of materials by reducing their grain size [49].

$$\sigma_y = \sigma_0 + kD^{-1/2} \qquad (1)$$

where σ_y is the yield stress, σ_0 is friction stress constant of the material (which depends on a lattice resistance of the material to the motion of dislocation) k is a constant and D is the average grain size. Due to the Hall-Petch relationship by reducing the grain size of the material to the nanosize, their strength increases considerably.

It is well established that nitrogen causes enhanced strength and hardness in nickel-free stainless steel and plays an essential role in grain size strengthening, which means nitrogen increases friction stress and the Hall-Petch slop [41]. The ductility of the HPF sample is 3% lower than the BAE sample. The reason for this behavior may be related to the higher number of dislocations that are created during the forging. The reason for the higher YS and UTS of the HPF sample than the BAE sample is related to the porosity content of these samples. The porosity reduces the strength and load-carrying capacity, so when the number of porosity decreases, UTS, and YS increase [50]. Gibson and Ashby suggested the mathematical model that describes the relationship between density and tensile strength according to Eq. (2) [51]:

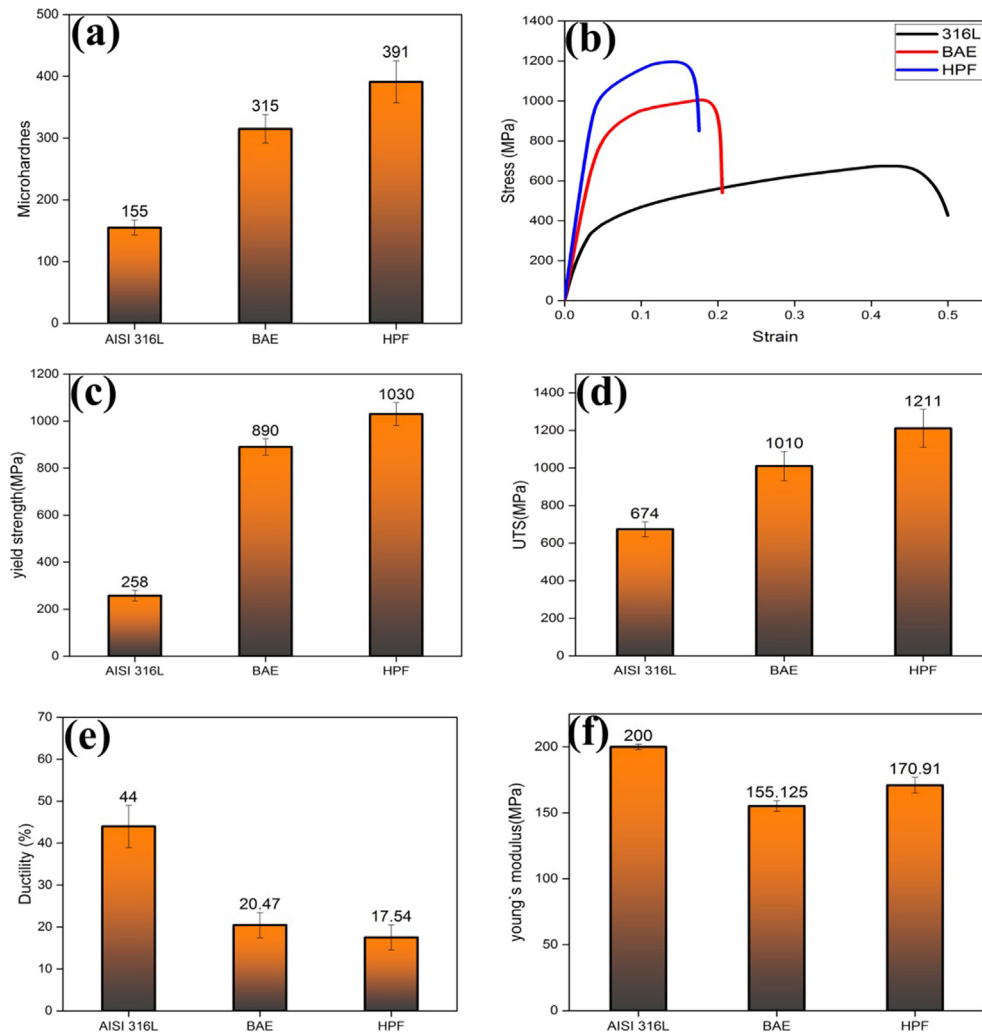$$\sigma/\sigma_0 = c(\rho/\rho_0)^n \qquad (2)$$

Fig. 7. A) Microhardnes of AISI 316L, BAE and HPF sample. B) The tensile test of BAE, HPF sample and 316L. C) Yield strength (YS) of AISI 316L, BAE and HPF sample. D) Ultimate tensile strength (UTS) of AISI 316L, BAE and HPF sample. E) Ductility of AISI 316L, BAE and HPF sample. F) Young's modulus of the AISI 316L, BAE and HPF sample.

where C and n are material constants that are dependent on the porous structure. ρ is the density of the porous sample, and ρ_0 is the density of the dense sample. According to the Ashley model, with increasing porosity, the tensile strength of the sample decreases. The porosity content also affects Young's modulus; Eq. (3) shows the relationship between Young's modulus (E) and porosity percentage [52]:

$$E = E_0\left((1 - \varepsilon)^2/1 + \varepsilon(2 - 3\gamma_0)\right) \qquad (3)$$

where E_0 is Young's modulus of the dense sample and E_0 for stainless steel nickel-free is 207 MPa, ε is the percentage of porosity, and γ_0 is Poisson's ratio constant, which is 0.305. According to Eq. (3), with an increasing percentage of porosity, Young's modulus decreases. The presence of nitrogen and manganese in austenitic stainless steel reduces Young's modulus. According to the theoretical model, the presence of nitrogen in the structure increases the interstitial sites and expansion of the unit cell [42] also elastic continuum models propose that the expansion of the unit cell decreases Young's modulus [48]. Fig. 7-f shows Young's modulus of the samples together with Young's modulus of an ordinary 316L stainless steel.

As shown in Fig. 7f, Young's modulus of samples fabricated by the HPF and BAE method is 17.45% and 28.5% less Young's modulus

of 316L stainless steel, respectively. This lower Young's modulus can be attributed to the effect of porosities that exist in the fabricated samples This contributes to a Young's modulus more similar to that of bone, which reduces the shielding effect [53]. Figs. 8 and 9 show the tensile fractured surfaces of HPF and BAE samples, respectively. Both specimens exhibit ductile fracture behavior consisting of dimple formation, growth of the voids and coalescence. The HPF fractured surface shows that in this specimen, the powders are thoroughly combined, and an integrated structure is created then, the fractured surface is covered with small and large voids with evidence of plastic deformation and coalescence of the voids. At the BAE fractured surface, lots of tiny dimples between large voids are observed; and it appears that large voids are produced by debonding of the powders from the surface. The ligament between the large voids is torn by the mechanism of dimple formation due to the plastic deformation of the ligament. Fig. 9 shows that the BAE specimen crack almost passed through the sintering aid additive between the powder particles, which indicates the bond between the powders is weaker in this specimen compared to the HPF.

According to our previous study on the press-sintered specimen, the sintering aid additive provides a better path for crack growth and, preventing crack growth toward the powder particles [39]. Since the sintering aid additive is the tougher phase, more
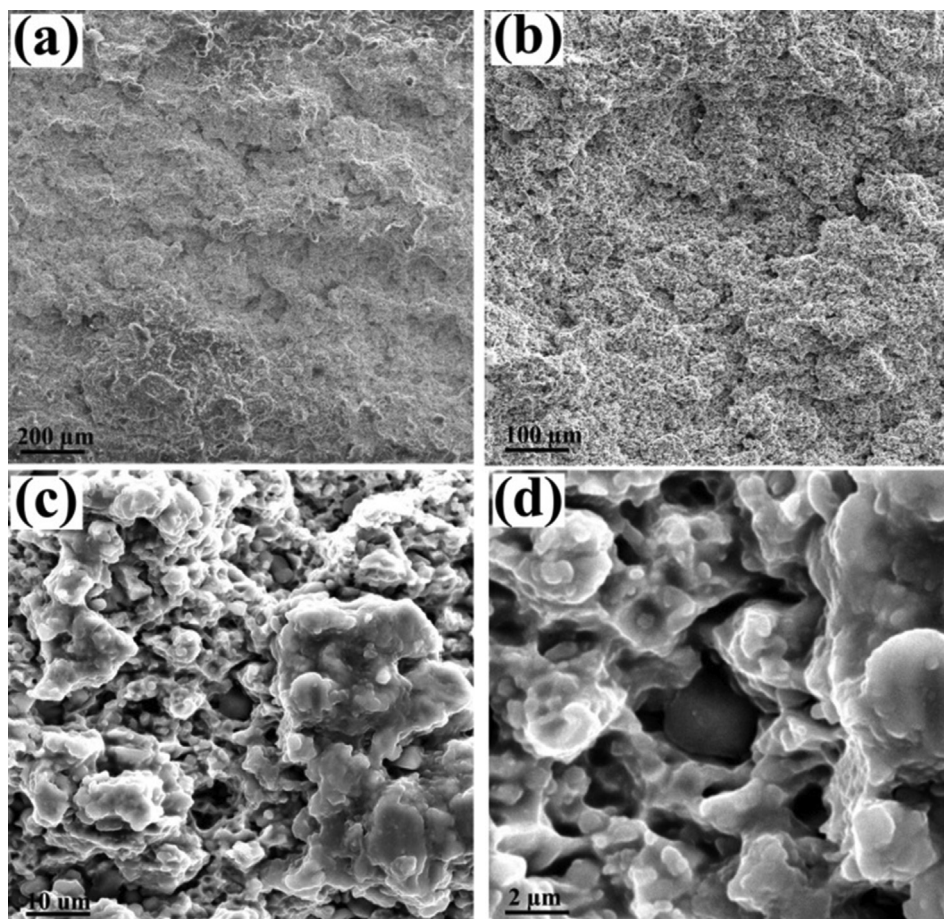
Fig. 8. The fractured surface of the tensile test of the HPF sample with various magnifications

plastic deformation occurs during crack growth in this phase and provides higher strain to failure for the BAE sample. Table 4 shows all the measured properties of the samples which are produced by the two fabrication methods.

Austenite stainless steels are fabricating in various methods, the most important of which are melting methods including electric arc melting (EAM), electroslag remelting (ESR), pressurized electroslag remelting (PSR), casting, nitrogen absorption treatment [54] and powder metallurgy methods including liquid phase sintering [37], BAE and HPF, etc. Alloys fabricated by melting methods often require secondary operations such as forming processes (forging or rolling) and machining, also require expensive equipment. The superior advantages of powder metallurgy methods over melting methods are provided near net shape product, achievable obtaining nano grain size, possible to introduce more nitrogen in the structure in the solid-state and with less expensive equipment, reduce production steps, and costs. Besides, the presence of cavities in the sample provides better cell adhesion for use in orthopedic implants.

A comparison of the published results to the results of the current study shows superior properties of the stainless steel produces by HPF and BAE over the most other methods. The results of a study on the properties of nickel-free stainless steel fabricated by pressure electro slag remelting showed yield strength of 590 MPa and the Ultimate strength of 1040 MPa. It has found that the alloy introduces better sliding behavior and corrosion resistance than ordinary stainless steel [55].

In another study, the mechanical properties of a high nitrogen nickel-free stainless steel fabricated by vacuum induction melting furnace followed by forging and rolling were investigated, and the results showed that the Ultimate Strength is about 941 MPa and is higher than the ordinary stainless steel [56].

Table 5 shows some other published data for some metals (stainless steels and others), which are using in biomaterials applications. A comparison of these data with results of the current study from Table 4 superior properties of the HPF and BAE is observed.

4. Conclusion

A nickel-free austenitic stainless steel was made by two fabrication routes—hot powder forging and binder assisted extrusion.

In the hot forging powder method, due to the simultaneous application of temperature and pressure, the sample reached 96% of theoretical density and obtained the strength with 3 times more than the strength of ordinary 316L stainless steel, along with greater hardness and very good ductility. Because of the high pressure applied during the hot powder forging, a large number of dislocations were formed in the samples, which result in the development of further sub-boundaries. So, this dislocation density together with a large number of dislocations produced during mechanical alloying provides a material with 38 nm crystalline size. The fracture surface of the sample shows a ductile fracture mechanism with a uniform structure that proves the porosities are filled.

In the binder assisted extrusion method, due to the use of a polymer binder, extrusion can be carried out at very low pressure (50 MPa) at room temperature. In this sense, this method is quite
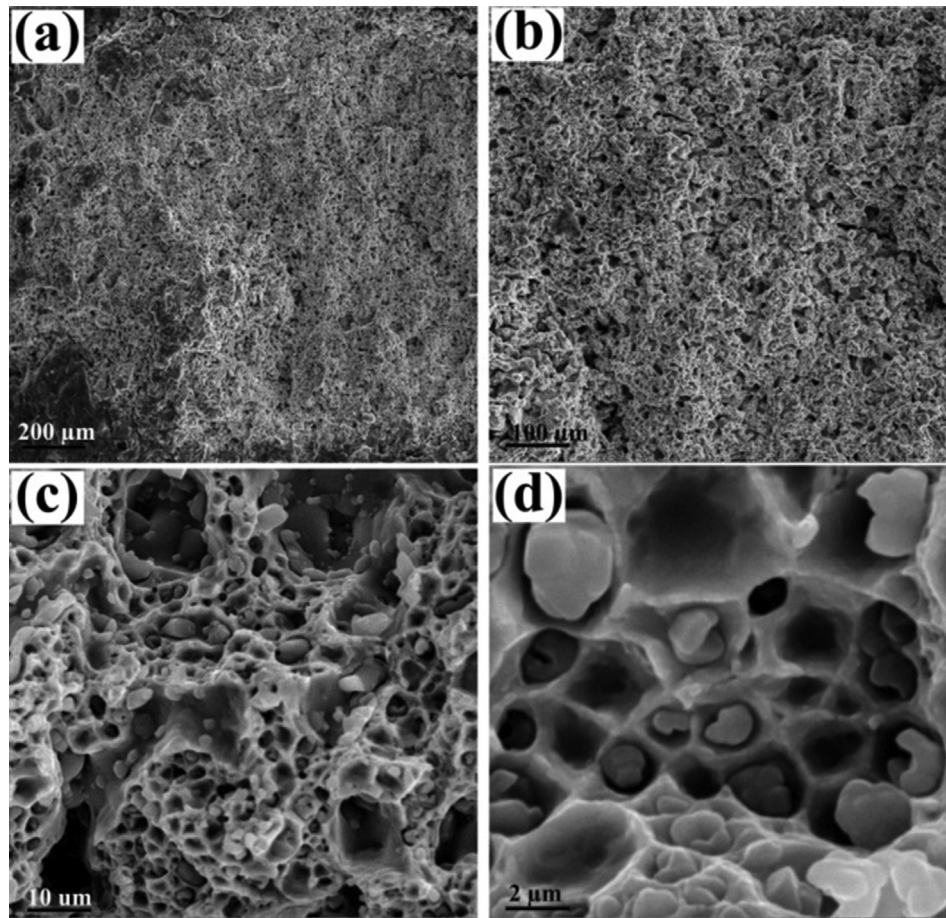
Fig. 9. The fracture surfaced of the tensile test of the BAE sample with different magnifications

Table 4
The measured properties of the samples produced by the two fabrication methods.

Sample	Microhardnes (HV)	Relative density (%)	UTS (MPa)	Yield strength (MPa)	Ductility (%)	Young modulus (MPa)	Porosity level (%)	Grain size (nm)
BAE	315	93	1010	890	20.47	155.125	9.21	90
HPF	391	96	1211	1030	17.54	170.91	6.8	62

Table 5
Mechanical properties of several metals used as orthopedic implants.

Material	Processing	Yield Strength (MPa)	Ultimate Strength (MPa)	Young's modulus (MPa)	Elon. (%)	Vickers hardness (H_V)	References
316L SS	Annealing	314	588	200	44	155	[57,4]
Rex 734(nickel-free stainless steels)	Annealing	584	898	–	39	289	[58]
Biodur 108(nickel-free stainless steels)	Hot Forging	586	931	–	52	–	[59]
F562 (Co-Ni-Cr-Mo)(nickel-free stainless steels)	Hot Forging	980	1210	230	–	–	[60]
BIOSSN4 (nickel-free stainless steels)	cast	559	938	–	54	248	[61]
Co31Cr4Mo (cobalt alloy)	Hot Isostatic Pressing	–	965	170	15	327	[62]
Ti-6Al-4V (titanium alloy)	cast	800	860	110	–	–	[63]

economical. After removing the binder and sintering, the density of samples rises to 93% of theoretical density. This specimen shows considerably higher strength and hardness than ordinary 316L stainless steel with very good ductility. specimens fabricated by this method exhibit lower strength and hardness but higher ductility compared to specimens produced by the hot forging powder method.

The fabricated samples show much higher strength than ordinary 316L stainless steel due to their nanostructure. The results have shown that both methods have produced a fully austenitic structure with nano-size grains. The density of HPF samples reached 3% higher than BAE samples, which results in an 8% higher Young's modulus of HPF than BAE samples. The results showed that despite the high hardness for the specimens made by powder

metallurgy, their Young's modulus was about 29 and 20% lower than Young's modulus of AISI316L, for BAE and HPF samples, respectively. This lower modulus is accounts for the existence of the porosity in the structure of the samples. This provides an advantageous feature for using these materials as orthopedic implants. Since the samples made by the HPF method found a finer structure than the BAE method, its yield stress and final strength are 13.5 and 20% higher than BAE, respectively. The comparison of the two methods shows that the forged specimens have higher strength and lower porosity than the samples fabricated by BAE. On the other hand BAE method produced material more easily with higher ductility.

Acknowledgment

References

[1] M.Z. Ibrahim, A.A.D. Sarhan, F. Yusuf, M. Hamdi, Biomedical materials and techniques to improve the tribological, mechanical and biomedical properties of orthopedic implants–A review article, J. Alloys Compd. 714 (2017) 636–667.

[2] D.J. Blackwood, Biomaterials: past successes and future problems, 2003.

[3] H. Hermawan, D. Ramdan, J.R.P. Djuansjah, Metals for biomedical applications, Biomed. Eng. Theory to Appl. (2011) 411–430.

[4] Q. Chen, G.A. Thouas, Metallic implant biomaterials, Mater. Sci. Eng. R Reports. 87 (2015) 1–57.

[5] M. Talha, C.K. Behera, O.P. Sinha, A review on nickel-free nitrogen containing austenitic stainless steels for biomedical applications, Mater. Sci. Eng. C. 33 (2013) 3563–3575.

[6] J.K.L. Lai, C.H. Shek, K.H. Lo, Stainless steels: An introduction and their recent developments, Bentham Science Publishers, 2012.

[7] U.K. Mudali, G. JB, P. Rodriguez, Pitting corrosion studies on nitrogen-bearing austenitic stainless steels, Mater. Trans. JIM. 37 (1996) 1568–1573.

[8] Y.S. Lim, J.S. Kim, S.J. Ahn, H.S. Kwon, Y. Katada, The influences of microstructure and nitrogen alloying on pitting corrosion of type 316L and 20 wt.% Mn-substituted type 316L stainless steels, Corros. Sci. 43 (2001) 53–68.

[9] J.Y. Park, S.-J. Park, J.-Y. Kang, C.-H. Lee, H.-Y. Ha, J. Moon, J.H. Jang, T.-H. Lee, Fatigue behaviors of high nitrogen stainless steels with different deformation modes, Mater. Sci. Eng. A. 682 (2017) 622–628.

[10] M.I.Z. Ridzwan, S. Shuib, A.Y. Hassan, A.A. Shokri, M.N.M. Ibrahim, Problem of stress shielding and improvement to the hip implant designs: a review, J. Med. Sci. 7 (2007) 460–467.

[11] T. Pohjonen, T. Lindgren, T. Puhakka, H. Happonen, A. Kaikkonen, Surgical implant and manufacturing method, 2007.

[12] C. Greiner, S.M. Oppenheimer, D.C. Dunand, High strength, low stiffness, porous NiTi with superelastic properties, Acta Biomater. 1 (2005) 705–716.

[13] C.S.Y. Jee, Z.X. Guo, J.R.G. Evans, N. Özgüven, Preparation of high porosity metal foams, Metall. Mater. Trans. B. 31 (2000) 1345–1352.

[14] K. Alvarez, K. Sato, S.K. Hyun, H. Nakajima, Fabrication and properties of Lotus-type porous nickel-free stainless steel for biomedical applications, Mater. Sci. Eng. C. 28 (2008) 44–50.

[15] M.T. Andani, N.S. Moghaddam, C. Haberland, D. Dean, M.J. Miller, M. Elahinia, Metals for bone implants. Part 1. Powder metallurgy and implant rendering, Acta Biomater. 10 (2014) 4058–4070.

[16] K.R. Vaidyanathan, J.L. Lombardi, J. Walish, R.A. Cipriani, Method for preparation of metallic foam products and products made, 2003.

[17] E. Ilia, M. O'Neill, K. Tutton, G. Lanni, S. Letourneau, M. Haehnel, Benchmarking the industry: powder forging makes a better connecting rod, SAE Trans. 340–352 (2005).

[18] S. Wang, Q. Wang, H.L. Wang, F.P. Liu, W.J. Yao, F. Jiang, J. Sun, F.Y. Wang, Effects of copper content on microstructure and mechanical properties of powder-forged rod Fe-C-Cu alloys manufactured at elevated temperature, Mater. Sci. Eng. A. 743 (2019) 197–206.

[19] M.H. Bocanegra-Bernal, Hot isostatic pressing (HIP) technology and its applications to metals and ceramics, J. Mater. Sci. 39 (2004) 6399–6420.

[20] P.J. James, Particle deformation during cold isostatic pressing of metal powders, Powder Metall. 20 (1977) 199–204.

[21] C.M. Sellars, G.J. Davies, Hot working and forming processes, in: Int. Conf. Organ. Jointly by Sheff. Metall. Eng. Assoc. Univ. Sheff. Assocation with Met. Soc., 1979.

[22] P.C. Angelo, R. Subramanian, Powder metallurgy: science, technology and applications, PHI Learning Pvt. Ltd., 2008.

[23] Z. Chen, K. Ikeda, T. Murakami, T. Takeda, Drainage phenomenon of pastes during extrusion, J. Mater. Sci. 35 (2000) 2517–2523.

[24] F. Händle, Extrusion in ceramics, Springer Science & Business Media, 2007.

[25] H. Takebe, M. Yoshida, K. Hayashi, K. Morinaga, Fabrication of alumina sheets by extrusion, J. Ceram. Soc. Japan. 100 (1992) 750–754.

[26] F. Händle, The Art of Ceramic Extrusion, Springer, 2019.

[27] H. Böhm, S. Blackburn, Agglomerate breakdown in fine alumina powder by multiple extrusion, J. Mater. Sci. 29 (1994) 5779–5786.

[28] M. Abdel-Rahman, M.N. El-Sheikh, Workability in forging of powder metallurgy compacts, J. Mater. Process. Technol. 54 (1995) 97–102.

[29] D.S. Li, Y.P. Zhang, X. Ma, X.P. Zhang, Space-holder engineered porous NiTi shape memory alloys with improved pore characteristics and mechanical properties, J. Alloys Compd. 474 (2009) L1–L5.

[30] E. Ilia, P. Plamondon, J.-P. Masse, G. L'Espérance, Copper precipitation at engine operating temperatures in powder-forged connecting rods manufactured with Fe–Cu–C alloys, Mater. Sci. Eng. A. 767 (2019) 138383.

[31] Y. Alshammari, F. Yang, L. Bolzoni, Mechanical properties and microstructure of Ti-Mn alloys produced via powder metallurgy for biomedical applications, J. Mech. Behav. Biomed. Mater. 91 (2019) 391–397.

[32] Z. Zhang, K. Frisk, A. Salwen, R. Sandström, Mechanical properties of Fe–Mo–Mn–Si–C sintered steels, Powder Metall. 47 (2004) 239–246.

[33] Q. Bai, J. Lin, J. Jiang, T.A. Dean, J. Zou, G. Tian, A study of direct forging process for powder superalloys, Mater. Sci. Eng. A. 621 (2015) 68–75.

[34] T. Tsutsui, Recent technology of powder metallurgy and applications, Hitachi Chem, Tech. Rep. (2012) 12.

[35] S.Z. Chavoshi, J. Jiang, Y. Wang, S. Fang, S. Wang, Z. Shi, J. Lin, Density-based constitutive modelling of P/M FGH96 for powder forging, Int. J. Mech. Sci. 138 (2018) 110–121.

[36] M. Javanbakht, M.J. Hadianfard, E. Salahinejad, Microstructure and mechanical properties of a new group of nanocrystalline medical-grade stainless steels prepared by powder metallurgy, J. Alloys Compd. 624 (2015) 17–21.

[37] M. Javanbakht, E. Salahinejad, M.J. Hadianfard, The effect of sintering temperature on the structure and mechanical properties of medical-grade powder metallurgy stainless steels, Powder Technol. 289 (2016) 37–43.

[38] E. Salahinejad, M.J. Hadianfard, M. Ghaffari, S.B. Mashhadi, A.K. Okyay, Liquid-phase sintering of medical-grade P558 stainless steel using a new biocompatible eutectic additive, Mater. Lett. 74 (2012) 209–212.

[39] E. Salahinejad, M.J. Hadianfard, M. Ghaffari, S.B. Mashhadi, A.K. Okyay, Fabrication of nanostructured medical-grade stainless steel by mechanical alloying and subsequent liquid-phase sintering, Metall. Mater. Trans. A. 43 (2012) 2994–2998.

[40] C. Suryanarayana, Mechanical alloying and milling, Prog. Mater. Sci. 46 (2001) 1–184.

[41] A. Di Schino, J.M. Kenny, Grain refinement strengthening of a micro-crystalline high nitrogen austenitic stainless steel, Mater. Lett. 57 (2003) 1830–1834.

[42] M.L.G. Byrnes, M. Grujicic, W.S. Owen, Nitrogen strengthening of a stable austenitic stainless steel, Acta Metall. 35 (1987) 1853–1862.

[43] K. Yamanaka, M. Mori, A. Chiba, Mechanical properties of as-forged Ni-free Co–29Cr–6Mo alloys with ultrafine-grained microstructure, Mater. Sci. Eng. A. 528 (2011) 5961–5966.

[44] H. Hänninen, J. Romu, R. Ilola, J. Tervo, A. Laitinen, Effects of processing and manufacturing of high nitrogen-containing stainless steels on their mechanical, corrosion and wear properties, J. Mater. Process. Technol. 117 (2001) 424–430.

[45] C.C. Koch, D.G. Morris, K. Lu, A. Inoue, Ductility of nanostructured materials, Mrs Bull. 24 (1999) 54–58.

[46] B.Q. Han, F.A. Mohamed, E.J. Lavernia, Tensile behavior of bulk nanostructured and ultrafine grained aluminum alloys, J. Mater. Sci. 38 (2003) 3319–3324.

[47] K. Huang, R.E. Logé, A review of dynamic recrystallization phenomena in metallic materials, Mater. Des. 111 (2016) 548–574.

[48] S. Cleja-Tigoiu, G.A. Maugin, Eshelby's stress tensors in finite elastoplasticity, Acta Mech. 139 (2000) 231–249.

[49] H. Li, Z. Jiang, Z. Zhang, Y. Yang, Effect of grain size on mechanical properties of nickel-free high nitrogen austenitic stainless steel, J. Iron Steel Res. Int. 16 (2009) 58–61.

[50] N. Chawla, X. Deng, Microstructure and mechanical behavior of porous sintered steels, Mater. Sci. Eng. A. 390 (2005) 98–112.

[51] M.F. Ashby, T. Evans, N.A. Fleck, J.W. Hutchinson, H.N.G. Wadley, L.J. Gibson, Metal foams: a design guide, Elsevier, 2000.

[52] L. Hu, T. Ngai, H. Peng, L. Li, F. Zhou, Z. Peng, Microstructure and properties of porous high-N Ni-free austenitic stainless steel fabricated by powder metallurgical route, Materials (Basel). 11 (2018) 1058.

[53] D.R. Sumner, Long-term implant fixation and stress-shielding in total hip replacement, J. Biomech. 48 (2015) 797–800.

[54] N. Maruyama, S. Hiromoto, E. Akiyama, M. Nakamura, Fretting fatigue behaviour of Ni-free high-nitrogen stainless steel in a simulated body fluid, Sci. Technol. Adv. Mater. 14 (2013) 25002.

[55] S. Koch, R. Büscher, I. Tikhovski, H. Brauer, A. Runiewicz, W. Dudzinski, A. Fischer, Mechanical, Chemical and Tribological Properties of the Nickel-free High-Nitrogen Steel X13CrMnMoN18-14-3 (1.4452), Materwiss. Werksttech. 33 (2002) 705–715.

[56] Y. Ren, P. Wan, F. Liu, B. Zhang, K. Yang, In vitro study on a new high nitrogen nickel-free austenitic stainless steel for coronary stents, J. Mater. Sci. Technol. 27 (2011) 325–331.

[57] U.I. Thomann, P.J. Uggowitzer, Wear–corrosion behavior of biocompatible austenitic stainless steels, Wear 239 (2000) 48–58.

[58] L. Kunčická, R. Kocich, T.C. Lowe, Advances in metals and alloys for joint replacement, Prog. Mater. Sci. 88 (2017) 232–280.

[59] D. Kuroda, T. Hanawa, T. Hibaru, S. Kuroda, M. Kobayashi, Mechanical properties and microstructures of a thin plate of nickel-free stainless steel with nitrogen absorption treatment, Mater. Trans. 44 (2003) 1363–1369.

[60] J.R. Davis, Handbook of materials for medical devices, 2003.

[61] Y. Ren, K. Yang, B. Zhang, Y. Wang, Y. Liang, Nickel-free stainless steel for medical applications, J. Mater. Sci. Technol. 20 (2004) 571–573.

[62] B. Henriques, M. Gasik, J.C.M. Souza, R.M. do Nascimento, D. Soares, F.S. Silva, Mechanical and thermal properties of hot pressed CoCrMo–porcelain composites developed for prosthetic dentistry, J. Mech. Behav. Biomed. Mater. 30 (2014) 103–110.

[63] C.-W. Lin, C.-P. Ju, J.-H.C. Lin, A comparison of the fatigue behavior of cast Ti–7.5 Mo with cp titanium, Ti–6Al–4V and Ti–13Nb–13Zr alloys, Biomaterials 26 (2005) 2899–2907.